Structure, mechanical properties, and grindability of dental Ti–Zr alloys

Wen-Fu Ho · Wei-Kai Chen · Shih-Ching Wu · Hsueh-Chuan Hsu

Abstract Structure, mechanical properties and grindability of a series of binary Ti–Zr alloys with zirconium contents ranging from 10 to 40 wt% have been investigated. Commercially pure titanium (c.p. Ti) was used as a control. Experimental results indicated that the diffraction peaks of all the Ti–Zr alloys matched those for α Ti. No β-phase peaks were found. The hardness of the Ti–Zr alloys increased as the Zr contents increased, and ranged from 266 HV (Ti–10Zr) to 350 HV (Ti–40Zr). As the concentration of zirconium in the alloys increased, the strength, elastic recovery angles and hardness increased. Moreover, the elastically recoverable angle of Ti–40Zr was higher than of c.p. Ti by as much as 550%. The grindability of each metal was found to be largely dependent on the grinding conditions. The Ti–40Zr alloy had a higher grinding rate and grinding ratio than c.p. Ti at low speed. The grinding rate of the Ti–40Zr alloy at 500 m/min was about 1.8 times larger than that of c.p. Ti, and the grinding ratio was about 1.6 times larger than that of c.p. Ti. Our research suggested that the Ti–40Zr alloy has better mechanical properties, excellent elastic recovery capability and improved grindability at low grinding speed. The Ti–40Zr alloy has a great potential for use as a dental machining alloy.

W.-F. Ho
Department of Materials Science and Engineering,
Da-Yeh University, Chang-Hwa, Taiwan, R.O.C

W.-K. Chen
Department of Mechanical and Automation Engineering,
Da-Yeh University, Chang-Hwa, Taiwan, R.O.C

S.-C. Wu · H.-C. Hsu (✉)
Department of Dental Laboratory Technology, Central Taiwan
University of Science and Technology, No. 11, Buzih Lane,
Beitun District, Taichung 40605, Taiwan, R.O.C
e-mail: hchsu@ctust.edu.tw

S.-C. Wu · H.-C. Hsu
Institute of Biomedical Engineering and Material Science,
Central Taiwan University of Science and Technology,
Taichung, Taiwan, R.O.C

1 Introduction

The use of commercially pure titanium (c.p. Ti) and its alloys in implants and prostheses is on the rise, largely because of their excellent biocompatibility, high strength to weight ratio, corrosion-resistance and low cost [1, 2]. Since the properties of unalloyed titanium are not strong enough for some dental purposes, many titanium alloys have been developed for dental use, and their properties have been studied [3–7], mainly to improve the strength and castability of pure titanium. Casting metals is not the only way to fabricate dental appliances. Recently, the CAD/CAM method represents a great advancement over casting technology [8]. However, the poor machinability of titanium is an obstacle to practical dental application. If titanium prostheses are fabricated by CAD/CAM, the tool life is short and the processing time is long [3, 9]. Although there may be several ways to improve grindability, one method is through alloying [10–14]. In any event, further development of new dental materials suited for machining is required.

For a metal to be used in a dental restoration, it should be biocompatible so that it does not cause harmful toxicological or allergic reactions to the patient. Among various titanium alloys, the Ti–6Al–4V alloy is the most widely used because of its better physical and mechanical properties in comparison to c.p. Ti [4]. However, there has

been speculation that the release of Al and V ions from the alloy might cause some long-term health problems [15–17]. Zirconium belongs to the IVB group in the periodic table, which is the same as titanium, and is known to have chemical properties similar to titanium. However, Ti–Zr alloys are also reported to have good corrosion resistance and biocompatibility [17, 18]. Therefore, these alloys could be candidates for dental prostheses. Another advantage of alloying zirconium to titanium is that the fusion temperature of the titanium (1,670°C) is lowered with an increase in the amount of zirconium (∼1,640°C for 10%Zr and 1,560°C for 40%Zr) [19], thus facilitating the casting process. Reducing the melting temperature of titanium could decrease its reactivity with oxygen and reduce the risk of inadequate mold filling and consequent porosity development which is due to the large temperature difference between the molten alloy and the much cooler investment [20].

Kobayashi et al. [21] investigated the mechanical properties of titanium–zirconium binary alloys through a hardness test, a tensile test, and optical microscopy. However, the machinability of the Ti–Zr alloys has not been investigated. In the present study, we investigate the structure and the mechanical properties by bending test for a series of binary Ti–Zr alloys with Zr contents up to 40 wt%. In addition, the grindability using an electric dental handpiece with SiC wheels was also evaluated, with the goal of developing a dental titanium alloy with better mechanical properties and machinability than c.p. Ti, a metal generally considered to be difficult to machine.

2 Materials and methods

The materials used for this study include c.p. Ti, Ti–10Zr, Ti–20Zr, Ti–30Zr, and Ti–40Zr alloys (in wt%). All the materials were prepared from raw titanium (99.8% in purity), Zr (99.95% in purity) using a commercial arc-melting vacuum–pressure-type casting system (Castmatic, Iwatani Corp., Japan). The melting chamber was first evacuated and purged with argon. An argon pressure of 1.5 kgf/cm^2 was maintained during melting. Appropriate quantities of Ti and Zr were melted in a U-shaped copper hearth with a tungsten electrode. The ingots were re-melted five times prior to casting to improve chemical homogeneity. Prior to casting, the ingots were melted once again in an open-based copper hearth under an argon pressure of 1.5 kgf/cm^2. The difference in pressure between the two chambers allowed the molten alloys to instantly drop into the graphite mold when melted. Compositions of the series of cast Ti–Zr alloys determined by scanning electron microscopy/energy dispersive spectrometry (SEM/EDS) are listed in Table 1.

Table 1 EDS-determined alloy compositions for the study

Alloy code	Zr (wt%)	Ti (wt%)
Ti–10Zr	9.28 ± 0.35	Balance
Ti–20Zr	19.42 ± 0.47	Balance
Ti–30Zr	27.61 ± 0.50	Balance
Ti–40Zr	36.66 ± 0.33	Balance

The cast alloys were sectioned using a Buehler Isomet low-speed diamond saw to obtain specimens. Surfaces of the alloys for microstructural study were mechanically polished via a standard metallographic procedure to a final level of 0.3 μm alumina powder and then etched in a solution of water, nitric acid, and hydrofluoric acid (80:15:5 in volume). The microstructure of the etched alloys was examined using an optical microscope (BH2, Olympus, Japan). X-ray diffraction (XRD) for phase analysis was conducted using a diffractometer (XRD-6000, Shimadzu, Japan) operated at 30 kV and 30 mA. A Ni-filtered CuKα radiation was used for this study. Phase was identified by matching each characteristic peak with the JCPDS files. The microhardness of polished alloys was measured using a microhardness tester (MVK-E3, Mitutoyo, Japan) at 100 g for 15 s.

Three-point bending tests were performed using a desktop mechanical tester (AG-IS, Shimadzu, Japan). The bending strengths were determined using the equation, $\sigma = 3PL/2bh^2$ [22], where σ is the bending strength (MPa), P is the load (kg), L is the span length (mm), b is the specimen width (mm), and h is the specimen thickness (mm). The dimensions of the specimens were: L = 30 mm, b = 5.0 mm, and h = 1.0 mm. The modulus of elasticity in bending is calculated from the load increment and the corresponding deflection increment between the two points on a straight line as far apart as possible using the equation: $E = L^3 \Delta P / 4bh^3 \Delta \delta$, where E is the modulus of elasticity in bending (Pa), ΔP is the load increment as measured from preload (N), and $\Delta \delta$ is the deflection increment at midspan as measured from preload. The average bending strength and modulus of elasticity in bending were taken from at least five tests under each condition. The elastic recovery (springback) capability for each material was evaluated from the change in deflection angle when loading was removed. The specimen is unloaded at the pre-set deflection of 8 mm. Details can be found in Ho et al. [23].

The method used in a previous study by several researchers [10–14, 24–26] was adopted to evaluate grindability in the present study. A silicon carbide (SiC) wheel (G11, Shofu, Kyoto, Japan) (diameter 13.1 mm, thickness 1.75 mm) on an electric dental handpiece (Ultimate 500, NSK Nakanishi Inc., Japan) was used to grind the specimens. Each specimen was placed on the test apparatus referred to in a previous study by

Ohkubo et al. [26] so that the edge of the wheel contacted one of the sidewalls of the rectangular specimen at 90°. By applying a force of 100 gf, the specimens were ground at one of the four rotational speeds of the wheel (500, 750, 1,000, or 1,200 m/min). The specimen and wheel were kept in a closed compartment during grinding so that the majority of the metal chips generated could be collected.

The amount of metal removed (mm^3) during 1 min was calculated from the density, previously measured using Archimedes' principle [26], and the weight loss of the specimen. A new wheel was applied for every test. The diameter and weight of each wheel were measured before and after grinding. Grindability was evaluated by volume of metal removed per minute (grinding rate) and the volume ratio of metal removed compared to the wheel material lost, which was calculated from the diameter loss (grinding ratio). The grinding rate represents ease of metal removal, whereas the grinding ratio is a measure of wheel life [13]. Three specimens were used to evaluate the grindability of each alloy; the test was performed twice for each kind of specimen at each grinding speed.

After testing, the ground surfaces of the metals were observed using optical microscopy (BH2, Olympus, Japan). The appearance of the chips resulting from the metal grinding was examined using an SEM (S-3000N, Hitachi, Japan). In this study, the experimental alloys were fabricated using a graphite mold instead of dental investment mold, which should not affect on findings. According to the results of Ohkubo et al. [26], there was no appreciable difference in the grindability between c.p. Ti with α-case and without α-case when an SiC wheel was used. All the results in this study were analyzed using one-way ANOVA and Duncan's multiple comparison test at $p < 0.05$ level.

3 Results and discussion

3.1 Microstructural characterization

The XRD patterns of the series of binary Ti–Zr alloys are shown in Fig. 1. For the Ti–Zr alloys, all the diffraction peaks matched well with those of α phase. There was no indication that β phase peaks or any intermediate phases were included in any of the present XRD patterns. The Ti–Zr system shows a completely solid solution for both high-temperature beta phase and low-temperature alpha phase [19]. This could partially explain why all the Ti–Zr alloys exhibit α phase. By comparison, due to the larger atomic radius of Zr (1.62 Å) than Ti (1.47 Å), the addition of Zr caused the α phase lattice parameters to increase, which in turn caused the XRD peaks to shift toward low-angle side. The higher the Zr content, the more obvious the shift was, as shown in the XRD patterns.
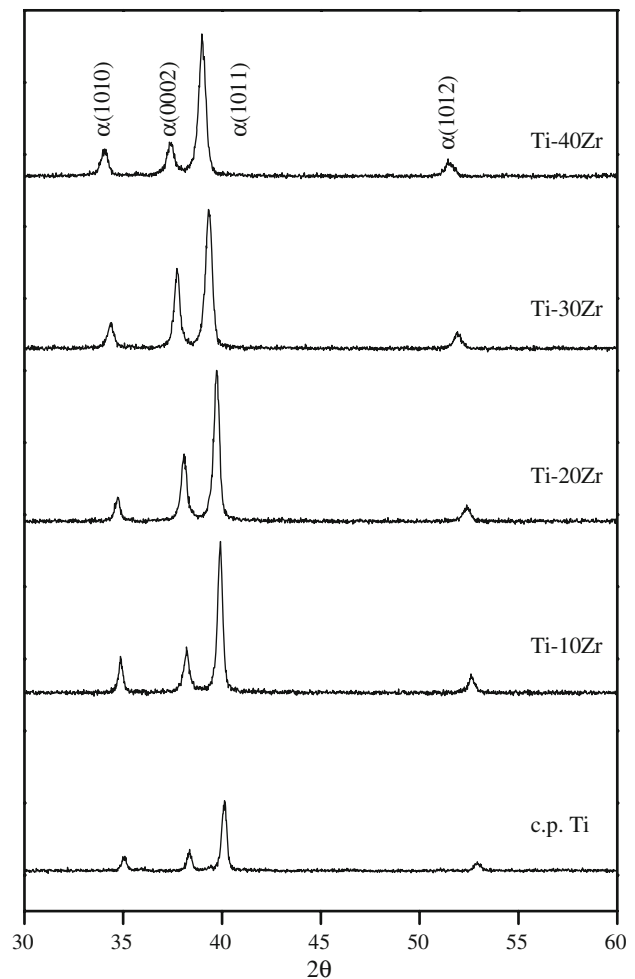

Fig. 1 XRD patterns of c.p. Ti and Ti–Zr alloys

Optical micrographs of the series of Ti–Zr alloys are shown in Fig. 2. All the Ti–Zr alloys showed hcp α structures and some martensitic structures. With increasing Zr content, the number of acicular, martensitic structures increased, probably as a result of a solute-induced decrease in Martensite transformation start (Ms) temperature [27]. Fineness of structure seemed to vary with alloy composition. The Ti–40Zr alloy exhibited the finest microstructure. The Ti–10Zr and Ti–20Zr alloys showed mainly facet type structures and the Ti–30Zr and Ti–40Zr alloys indicated some needle type structures. These facet- and needle-like structures are caused by some diffusionless transformation during cooling [21].

3.2 Mechanical properties

Microhardness values of the Ti–Zr alloys are shown in Fig. 3. The hardness of c.p. Ti was 186 HV. The hardness of the Ti–Zr alloys increased as the Zr contents increased, and ranged from 266 (Ti–10Zr) to 350 HV (Ti–40Zr).

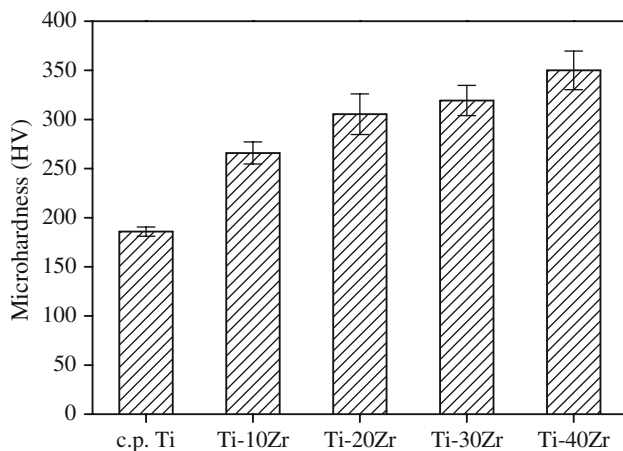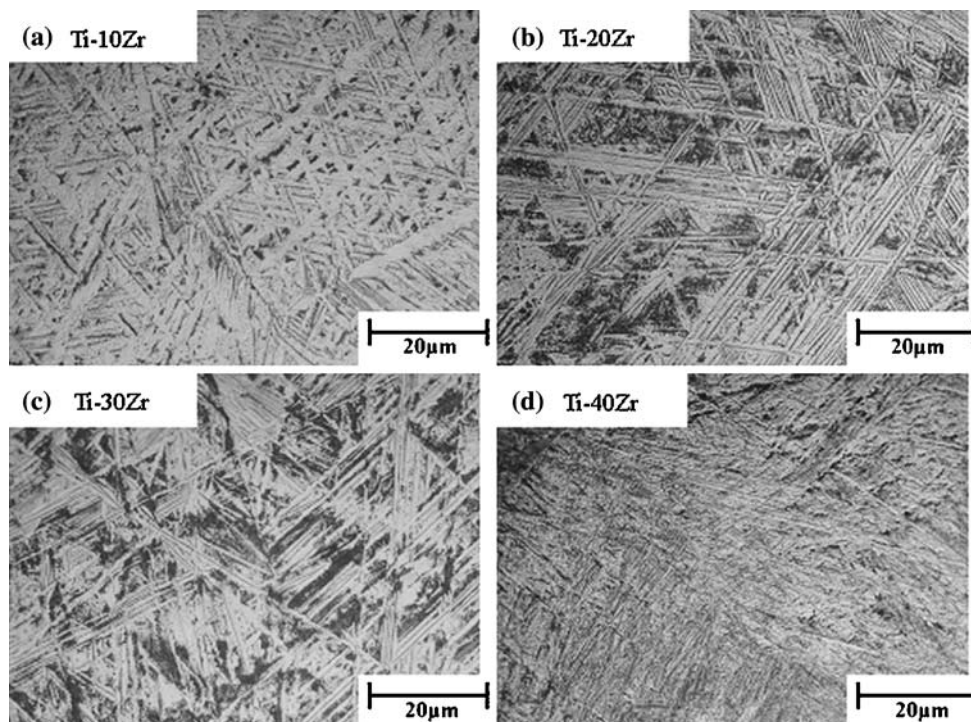**Fig. 2** Optical micrographs of Ti–Zr alloys

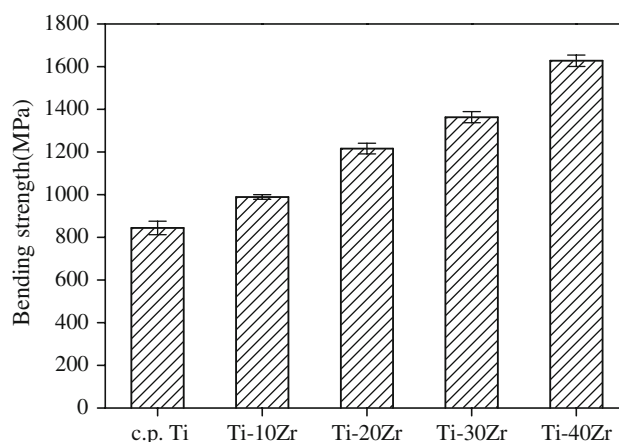**Fig. 3** Microhardness of c.p. Ti and Ti–Zr alloys

Fig. 4 Bending strengths of c.p. Ti and Ti–Zr alloys

ANOVA test results showed significant overall differences among microhardness values for c.p. Ti and Ti–Zr alloys ($p < 0.05$). All the Ti–Zr alloys had significantly higher ($p < 0.05$) hardness than the c.p. Ti tested. Since the Ti–Zr alloys exhibit complete solid solution, their hardness values showed continuous change throughout the system. The Ti–40Zr alloy showed the highest hardness value, which was probably caused by the solid-solution hardening of α phase and the contribution of the finest microstructure.

The bending strengths of all the Ti–Zr alloys (989–1,628 MPa) were significantly higher ($p < 0.05$) than that of c.p. Ti (844 MPa), as shown in Fig. 4. The bending strengths of the Ti–Zr alloys increased proportionately with an increasing Zr content. Of the Ti–Zr alloys, the alloy with 40 wt% Zr content shows the highest bending strength. The bending strength of the Ti–40Zr alloy was about two times greater than for c.p. Ti. Similarly, Nakasuji and Okada [28] also reported that the tensile strengths and yield strengths of Ti–Zr alloys with Zr concentrations of up to 20 wt% were increased as the Zr contents increased.

The bending moduli of the Ti–Zr alloys are shown in Fig. 5. The bending moduli of all the Ti–Zr alloys are significantly higher ($p < 0.05$) than that of c.p. Ti. Although the alloy phase of the Ti–Zr alloys was a single α phase, their elastic moduli decreased as the concentration of Zr increased. One possible explanation for this is that the
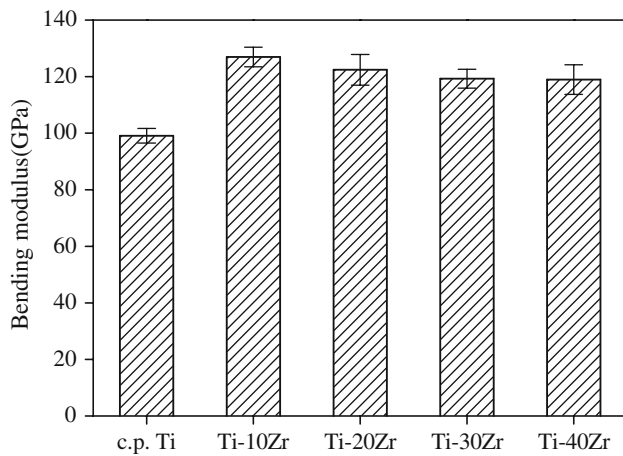
Fig. 5 Bending moduli of c.p. Ti and Ti–Zr alloys

crystal structure of α titanium was slightly changed by alloying with Zr. Based on the Duncan's test, there was no significant difference in the bending modulus among Ti–20Zr, Ti–30Zr, and Ti–40Zr alloys.

Figure 6 shows that the means of the elastic recovery capability of Ti–Zr alloys increased as the concentration of Zr increased. ANOVA test results showed significant overall differences among elastic recovery angles for c.p. Ti and Ti–Zr alloys ($p < 0.05$). All the Ti–Zr alloys had significantly higher ($p < 0.05$) elastic recovery angles than the c.p. Ti tested. This trend is similar to that of hardness or strength. It is worth noting that the advantage in mechanical properties of Ti–40Zr alloy is also demonstrated in its high elastic recovery capability. High elastic recovery (springback) capability of a metal is an indication of high strength and low modulus [23, 29–31], and is essential for many load-bearing implant and dental applications. The elastic recovery capability of Ti–40Zr alloy was greater than all other Ti alloys fabricated in this study. For
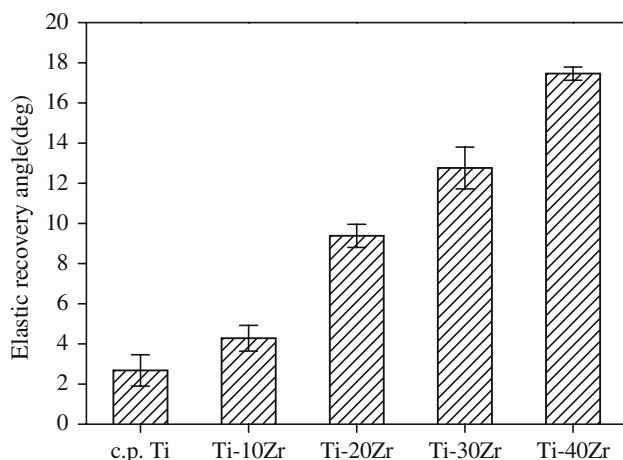
example, the elastically recoverable angle of Ti–40Zr alloy was higher than that of c.p. Ti by as much as 550%.

As the concentration of Zr in the alloys increased, the strengths, elastic recovery angles and hardness values all increased. According to the equilibrium phase diagram for the binary Ti–Zr alloy [19], no intermetallic compound is formed. Therefore, changes in the mechanical properties produced by alloying were probably caused by solid-solution strengthening of the phases. The solid solution mechanism would result in greater resistance to the slip system [32]. These results are similar to those of the Ti–Nb alloy system reported by Kikuchi et al. [10]. The mechanical properties of the alloys were strongly affected by the concentration of alloying elements and by the grain refinement.

3.3 Grindability

The grinding rates of the Ti–Zr alloys at four different grinding speeds are shown in Fig. 7a. Up to a grinding speed 1,200 m/min, the grinding rates of c.p. Ti, Ti–10Zr, and Ti–20Zr showed a tendency to increase as the grinding

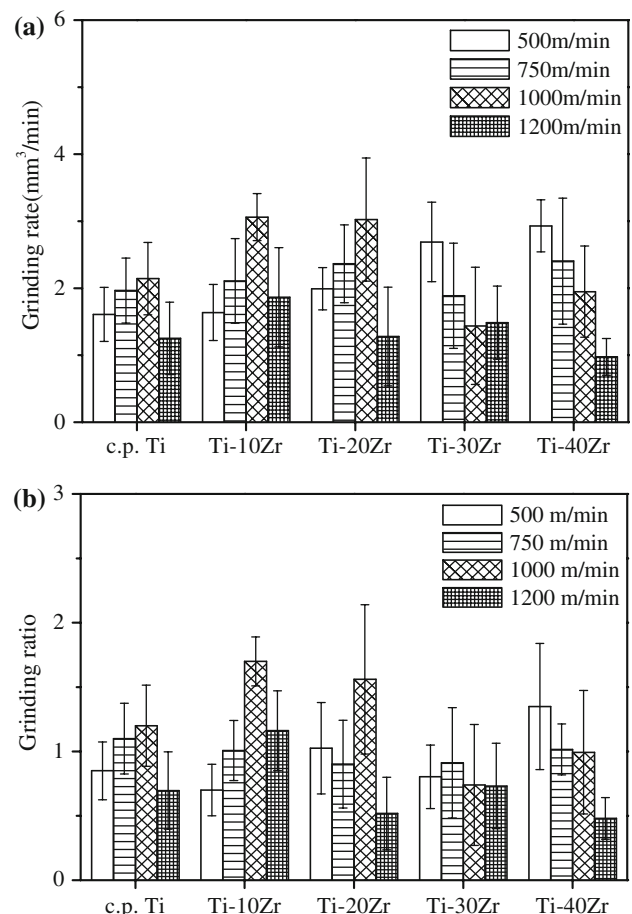Fig. 6 Elastic recovery angles of c.p. Ti and Ti–Zr alloys

Fig. 7 Grindability of c.p. Ti and Ti–Zr alloys. (a) Grinding rate, (b) Grinding ratio

speed increased. In contrast, the grinding rates of Ti–30Zr and Ti–40Zr decreased as the grinding speed increased. At the grinding speed of 500 m/min, the rates for the Ti–30Zr and Ti–40Zr alloys were significantly higher than those of the other metals tested ($p < 0.05$). The grinding rate of the Ti–40Zr alloy at 500 m/min was about 1.8 times higher than that of c.p. Ti. At the grinding speed of 1,000 m/min, the rates for the Ti–10Zr alloy were significantly higher than those of the other Ti–Zr alloys tested ($p < 0.05$). However, at 1,200 m/min, the rates of all the Ti–Zr alloys and c.p. Ti decreased. It is worth noting that all the metals in this study had the lowest grinding rates at the highest speed, 1,200 m/min. Similar results can be found in other titanium alloy systems [13]. Although further study is needed, it is possible that the condition of the grinding wheel deteriorates at the speed of 1,200 m/min.

The grinding ratios of the Ti–Zr alloys are shown in Fig. 7b. The grinding ratios had a similar tendency to the grinding rates as the grinding speed increased. At 1,000 m/min, the Ti–10Zr alloy exhibited a significantly higher grinding ratio than did the Ti–30Zr, Ti–40Zr, and c.p. Ti ($p < 0.05$). The grinding ratio of the Ti–10Zr alloy at 1,000 m/min was about 1.4 times higher than that of c.p. Ti. Moreover, at 500 m/min, the Ti–40Zr alloy had a significantly higher grinding ratio than did all the other Ti–Zr and c.p. Ti ($p < 0.05$). The grinding ratio of the Ti–40Zr alloy at 500 m/min was about 1.6 times higher than that of c.p. Ti. With respect to grinding ratio, all the metals had the lowest values at the highest speed, 1,200 m/min. However, the Ti–10Zr alloy still had a significantly higher grinding ratio than did c.p. Ti and all the other Ti–Zr alloys ($p < 0.05$). Tool life can be predicted based on an evaluation of the grinding ratio. A higher grinding ratio signifies lower tool wear for the same volume of metal removed [13]. The ratios varied widely for all the metals tested, probably because both the volumes of the metal ground and wheel material lost were very small.

Takeyama [33] showed that higher strength and hardness of a material generally make machining of the material more difficult. In the present study, at the speed of 1,000 m/min the grinding of the Ti–Zr alloys became more difficult with higher Zr contents, which exhibit higher hardness. However, the Ti–40Zr alloy had a higher grinding rate than Ti–10Zr at a low speed. In early studies, some researchers [34–36] discussed grindability in terms of the relationship between the hardness of the metals. Nevertheless, in the present study there appeared to be no correlation between the volume loss and the hardness of the metals. This result was also in agreement with that reported by Ohkubo et al. [26] who tested c.p. Ti and Ti–6Al–4V alloy. It seems that hardness and strength are not the principal reasons for the better grindability.

According to Kikuchi et al. [10], elastic modulus seemed to have no relation with grindability. Nevertheless,

the relatively low elastic modulus of titanium causes chatter vibration or deformation of the workpiece during machining [37]. Kikuchi et al. [10] suggested that the titanium alloys with higher elastic modulus than c.p. Ti are more favorable for machining. In the present study, all the Ti–Zr alloys had higher elastic modulus than that of c.p. Ti. Therefore, with respect to modulus, the Ti–Zr alloys are more suitable for dental machining alloys.

3.4 Observation of metal chips and ground surfaces

Typical metal chips that resulted from grinding at 500 and 1000 m/min are shown in Fig. 8. Although no quantitative analysis was performed, the size of the metal chips of c.p.
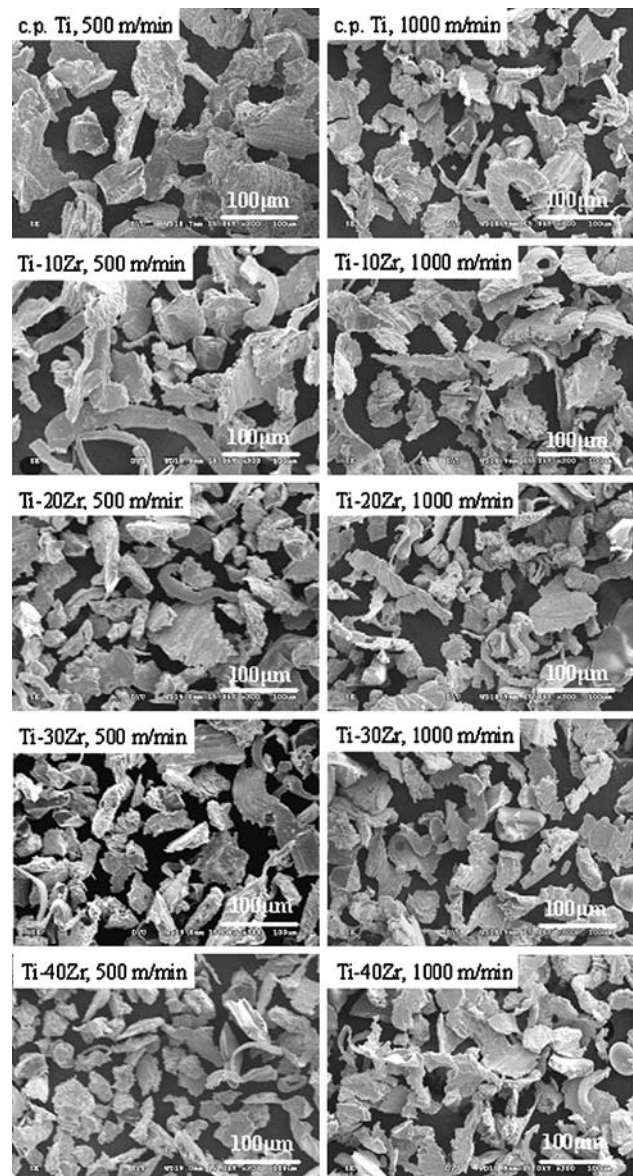

Fig. 8 SEM micrographs of metal chips from grinding at 500 and 1,000 m/min

Ti at 500 m/min generally appeared somewhat larger than those of Ti–Zr alloys. The finer metal chips are more suitable for grinding than larger metal chips [14]. For the Ti–30Zr and Ti–40Zr alloys, the size of the metal chips appears to be larger at a grinding speed of 1,000 m/min than that at 500 m/min. This result might be related to their higher grinding rate at 500 m/min.

Figure 9 shows optical micrographs of the ground surfaces of the metals at 500 and 1,000 m/min. Grinding marks were observed for all the metals and speeds. There was no pronounced difference in the appearance of the ground surface among Ti–Zr alloys at 500 m/min, except for a few grinding adhesion on the ground surface of c.p. Ti. Grinding adhesion of metal was observed to a greater degree for c.p. Ti, Ti–10Zr, and Ti–20Zr alloys ground at

1,000 m/min. In contrast, grinding burns could be found on Ti–30Zr and Ti–40Zr alloys at 1,000 m/min. As mentioned in the literature [11, 12, 14], the grinding burn typically found on titanium and titanium alloys results from high-speed grinding. In addition, appreciable sparking was occasionally observed during the grinding test, especially at a high grinding speed.

4 Conclusions

The following conclusions can be drawn from this study:

(1) Based on the results of XRD and optical microscopy, all the Ti–Zr alloys showed hcp α structures.

Fig. 9 Grinding surfaces of c.p. Ti and Ti–Zr alloys at 500 and 1,000 m/min
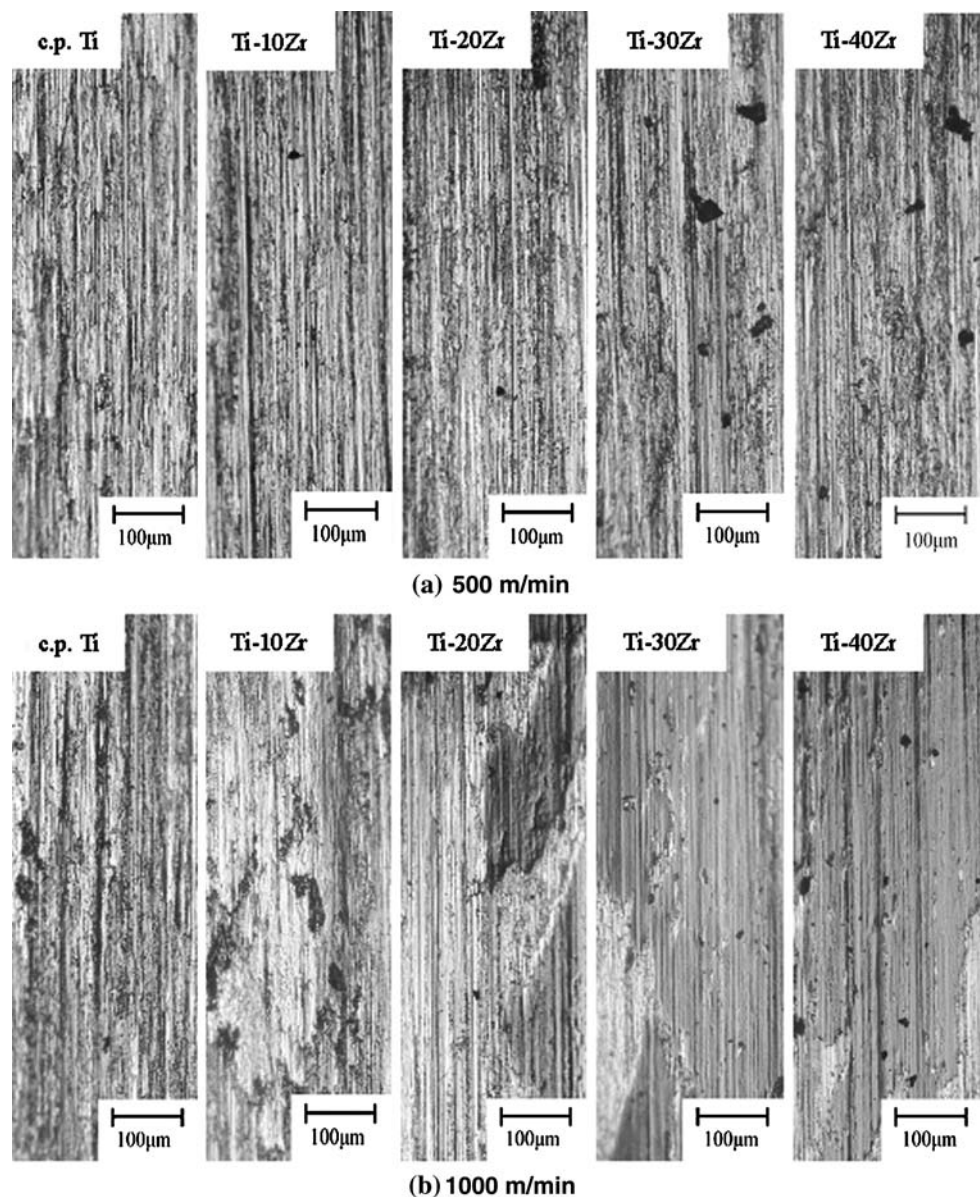
(2) All the Ti–Zr alloys had higher microhardness values, bending strengths, bending moduli and elastic recovery angles than those of c.p. Ti. The microhardness value of Ti–40Zr was higher than that of c.p. Ti by 88%. The bending strength of Ti–40Zr was higher than that of c.p. Ti by 93%. Furthermore, the elastically recoverable angle of Ti–40Zr was higher than that of c.p. Ti by as much as 550%.

(3) At the higher grinding speed of 1,000 m/min, the Ti–10Zr and Ti–20Zr alloys exhibited better grindability than c.p. Ti. On the other hand, at the lower grinding speed of 500 m/min, the grinding rates for the Ti–30Zr and Ti–40Zr alloys were notably higher than that of c.p. Ti.

References

1. R.R. Wang, A. Fenton, Quintessence Int. **27**, 401 (1996)
2. J.A. Hautaniemi, H. Hero, J.T. Juhanoja, J. Mater. Sci. **3**, 186 (1992)
3. O. Okuno, H. Hamanaka, Dent. Jpn. **26**, 101 (1989)
4. E.P. Lautenschlager, P. Monaghan, Int. Dent. J. **43**(3), 245 (1993)
5. M. Hattori, K. Hasegawa, M. Yoshinari, E. Kawada, Y. Oda, T. Okabe, Dent. Mater. J. **20**(1), 16 (2001)
6. Y. Takada, H. Nakajima, O. Okuno, T. Okabe, Dent. Mater. J. **20**(1), 34 (2001)
7. M. Takahashi, M. Kikuchi, Y. Takada, O. Okuno, Dent. Mater. J. **21**(3), 270 (2002)
8. F. Duret, J.L. Blouin, B. Duret, J. Am. Dent. Assoc. **117**(6), 715 (1988)
9. H. Nakajima, T. Okabe, Dent. Mater. J. **15**, 77 (1996)
10. M. Kikuchi, Y. Takada, S. Kiyosue, M. Yoda, M. Woldu, Z. Cai, O. Okuno, T. Okabe, Dent. Mater. **19**, 375 (2003)
11. M. Kikuchi, M. Takahashi, T. Okabe, O. Okuno, Dent. Mater. J. **22**(2), 191 (2003)
12. M. Kikuchi, M. Takahashi, O. Okuno, Dent. Mater. J. **22**(3), 328 (2003)
13. M. Kikuchi, M. Takahashi, H. Sato, O. Okuno, M.E. Nunn, T. Okabe, J. Biomed. Mater. Res. B., Appl. Biomater. **77**(1), 34 (2005)
14. M. Takahashi, M. Kikuchi, O. Okuno, Dent. Mater. J. **23**(2), 203 (2004)
15. P.R. Walker, J. Leblanc, M. Sikorska, Biochemistry **28**, 3911 (1989)
16. S. Yumoto, H. Ohashi, H. Nagai, S. Kakimi, Y. Ogawa, Y. Iwata, K. Ishii, Int. J. PIXE **2**, 493 (1992)
17. Y. Okazaka, S. Asao, S. Rao, T. Tateshi, J. Jpn. Inst. Met. **60**(9), 902 (1996)
18. D.L. Douglass, At. Energy Rev. **3**, 71 (1963)
19. J.L. Murray, Binary alloy phase diagrams, in *Alloy Phase Diagrams*, ed. by H. Baker (ASM International, Materials Park, OH, 1987), p. 340
20. S. Zinelis, A. Tsetsekou, T. Papadopoulos, J. Prosth. Dent. **90**, 332 (2003)
21. E. Kobayashi, S. Matsumoto, H. Doi, T. Yoneyama, H. Hamanaka, J. Biomed. Mater. Res. **29**, 943 (1995)
22. A. Guha, in *Metals Handbook*, 9th edn (ASM International, Materials Park, OH, 1985), p. 133
23. W.F. Ho, C.P. Ju, J.H. Chern Lin, Biomaterials **20**, 2115 (1999)
24. M. Taira, M. Okazaki, J. Takahashi, M. Yamaki, J. Oral Rehabil. **24**(7), 527 (1997)
25. I. Watanabe, C. Ohkubo, J.P. Ford, M. Atsuta, T. Okabe, Dent. Mater. **16**(6), 420 (2000)
26. C. Ohkubo, I. Watanabe, J.P. Ford, H. Nakajima, T. Hosoi, T. Okabe, Biomaterials **21**, 421 (2000)
27. J.C. Willians, Critical review: kinetics and phase transformation, in *Titanium Science and Technology; Proceeding* (Metallurgical Society of AIME, Plenum Press, New York, 1973), p. 1433
28. K. Nakasuji, M. Okada, Mater. Sci. Eng. **A213**, 162 (1996)
29. W.J. Gammon, O. Kraft, A.C. Reilly, B.C. Holloway, Carbon **41**, 1917 (2003)
30. C.W. Lin, C.P. Ju, J.H. Chern Lin, Biomaterials **26**, 2899 (2005)
31. W.W. Cheng, C.P. Ju, J.H. Chern Lin, J. Oral Rehabil. **34**, 528 (2007)
32. A.G. Guy, *Introduction to Materials Science* (McGraw-Hill, New York, 1972), p. 225
33. H. Takeyama, T. Yoshikawa, J. Takada, J. Jpn. Soc. Preci Eng. **41**(4), 392 (1975)
34. R. Grajower, I. Kurz, M.S. Bapna, Dent. Mater. **2**, 187 (1986)
35. M.H. Reisbick, B.F. Bunshah, J. Dent. Res. **52**, 1138 (1973)
36. W.J. O'brien, *Dental Materials Properties and Selection*, 3rd edn (Quintessence Publishing Co, Chicago, 1989), p. 515
37. E.O. Ezugwu, Z.M. Wang, J. Mater. Process. Tech. **68**(3), 262 (1997)